J Solid State Electrochem (2002) 6: 172–182
DOI 10.1007/s100080100218

ORIGINAL PAPER

L.C. Roland Alfred · Jan C. Myland · Keith B. Oldham

Corrosion current densities at a disk-shaped inclusion

Received: 16 November 2000 / Accepted: 2 April 2001 / Published online: 19 October 2001

Abstract Laplace's equation is solved for the geometry of a polarized disk, of radius R, inlaid in a coplanar conductor and immersed in an aqueous electrolyte solution of conductivity κ. This geometry corresponds to a corroding inclusion on the surface of a metal sheet when the rate of corrosion is controlled by ohmic polarization. When the corrosion potential is Φ, the corrosion current density is found to have a minimum anodic value, equal to $\kappa\Phi/R$, in the centre of the disk. Current densities at a variety of sites on the disk-shaped anode and on the annular cathode have been determined numerically. Limiting behaviours have also been delineated. Equipotential surfaces are portrayed in a cross-sectional diagram, which also shows the routes taken by the corrosion current. The behaviour of the current in special regions – near the axis, near the three-phase junction and on remote regions of the cathode – can be described by simple formulas.

Keywords Corrosion · Disk · Inclusion · Laplace equation

Introduction

A small region of atypical composition, known as an "inclusion", on the surface of an inhomogeneous alloy can be the site of corrosion when the metal is in contact with an aqueous solution. If the inclusion is more noble than the surrounding metal, the latter will serve as the anode in a corrosion cell. An example of this situation arises when copper-rich inclusions are present on the surface of structural aluminium alloys. The inclusion then serves as a cathode at which an electroreduction, typically of dissolved oxygen, occurs. The concomitant anodic corrosion occurs over the much larger area of the surrounding annulus and metal dissolution is widespread. More dramatic in the corrosion effect is the case in which the inclusion is less noble than the metal surrounding it. Because the small anode is coupled to a much larger cathode, the localized corrosion can be intense and a pit may develop on the metal surface. Though the treatment of a cathodic inclusion is strictly analogous, we shall adopt signs in this article that correspond to the inclusion serving as an anode. Figure 1a is a cross-sectional diagram of an anodic inclusion, showing the paths taken by ions and electrons to sustain the corrosion cell. Employing the scanning vibrating electrode technique [1, 2, 3], He and coworkers [4, 5] have mapped the ionic current densities in the vicinity of a corroding inclusion by determining the distribution of the electric field in the surrounding solution. One object of the present study is to provide a theoretical basis with which to compare such experimental results. One such comparison has already been published [6].

L.C.R. Alfred · J.C. Myland · K.B. Oldham (✉)
Trent University, Peterborough, Ontario K9J 7B8, Canada
E-mail: koldham@trentu.ca
Tel.: +1-705-748-1011 x1336
Fax: +1-705-748-1625

The model

In this article, a corrosion cell arising from a disk-shaped anodic inclusion is modelled in the steady state. Thus, a constant positive corrosion current, I, is postulated to flow ionically from the disk to the surrounding metal through the electrolyte solution and electronically from the annulus to the disk through the metal. A major objective of the present study is to calculate the magnitudes, j, of the corresponding current densities on the metal surfaces; these will vary from point to point and will be positive on the disk but negative on the surrounding infinite annulus. The corrosion arises from a chemical potential difference between the inclusion and the alloy of typical composition. If x_{incl} and x_{surr} represent the mole fractions of the base metal in the inclusion and in the surrounding surface alloy, respectively,

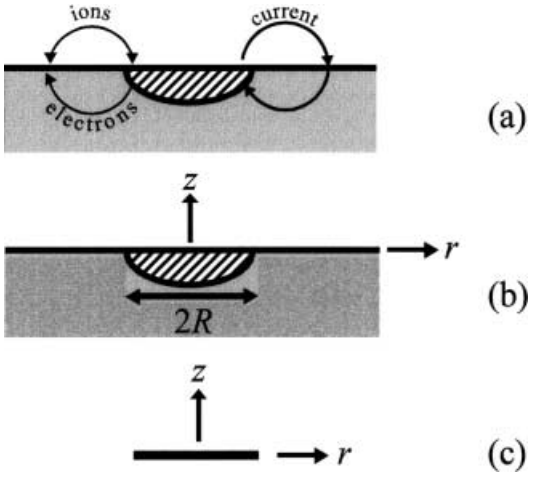

Fig. 1 **a** The routes taken by current, ions and electrons in the anodic corrosion of an inclusion. **b** The cylindrical coordinates initially employed. **c** The mathematically equivalent geometry of a dipolar disk

then the chemical potential difference will be parlayed into an electrical potential difference of

$$\Phi = \frac{RT}{n_e F} \ln\left\{\frac{x_{\text{incl}}}{x_{\text{surr}}}\right\} \tag{1}$$

where other symbols have their standard electrochemical significance. This formula assumes that the inclusion and the bulk alloy behave as ideal solid solutions, an assumption that might sometimes be grossly incorrect. The potential Φ, which will be positive if the inclusion is relatively base as assumed here, exists at the surface of the inclusion, with respect to the surface of the surrounding metal, to which a potential of zero is arbitrarily assigned.

The power ΦI created by the corrosion cell is dissipated in overcoming three possible impediments to current flow: activation polarization, concentration polarization and ohmic polarization. Activation polarization arises from any irreversibilities in the electrode reactions. Concentration polarization has its origin in nonuniformities in the composition of the solution bathing the electrode sites. Ohmic polarization arises from the need to force ionic current through the aqueous solution, a resistive medium. It will be assumed that activation polarization is absent. Because the aqueous solution is taken to have a uniform and constant composition, concentration polarization will also be discounted. Thus, the model takes cognizance only of ohmic polarization arising from the uniform finite conductivity, κ, of the aqueous medium. Also ignored are any impediments to current flow that might arise from films on the surface of the metal or in the electron pathway. Because the many effects that are being ignored may often be comparable with, or overwhelm, ohmic polarization, the results of this study should be regarded as a prediction of the *maximum* corrosion current densities that can exist.

Cell geometry

The geometry that will be assumed is of an inclusion forming a circular disk-shaped anode on the surface of the metal sample, the cathode being the infinite coplanar annulus surrounding the disk. The aqueous solution is semiinfinite in extent, occupying all the space corresponding to $0 \le z < \infty$ in the cylindrical coordinate system depicted in Fig. 1b. The anode is defined geometrically by $z = 0$, $r < R$ and the cathode by $z = 0$, $r > R$. The hoop $z = 0$, $r = R$ represents a three-phase junction at which the anode, cathode and solution all meet; it can be confidently anticipated that the corrosion current will have an infinite density there.

As prescribed by this model, the problem devolves into first finding the potential $\phi\{r,z\}$ at all points in the space occupied by the aqueous solution, by solving Laplace's equation

$$\nabla^2\phi = \frac{\partial^2\phi}{\partial r^2} + \frac{1}{r}\frac{\partial\phi}{\partial r} + \frac{\partial^2\phi}{\partial z^2} = 0 \tag{2}$$

subject to the boundary conditions

$$\phi\{r,0\} = \Phi \quad r < R \tag{3}$$

and

$$\phi\{r,0\} = 0 \quad r > R. \tag{4}$$

Once the solution to that problem is found, the local current density, $j\{z,r\}$, can then be determined from Ohm's law in the form $j = -\kappa(\partial\phi/\partial n)$, where n is the normal to the equipotential surface at the point in question. On both the anode and the cathode, this normal coincides with the z-coordinate and therefore

$$j(r,\ 0) = -\kappa\frac{\partial\phi}{\partial z} \tag{5}$$

permits the current density to be calculated. We expect $j(r,0)$ to be positive at $r = 0$, to increase dramatically as r approaches R, to suffer an infinite discontinuity at $r = R$, to be negative for $r > R$ and to approach zero as $r \to \infty$. It will transpire that this expectation is realized, as a glance at Fig. 3 will confirm.

Because the flux lines will be normal to the $z = 0$ plane, for r both smaller than and larger than R, a mathematically equivalent problem is the following. An infinitely thin circular disk of radius R is immersed in an infinite medium of uniform conductivity κ, as depicted in Fig. 1c. Solve Laplace's equation if one face of the disk is held at a potential Φ and the other at potential $-\Phi$. Considerations of symmetry then ensure that condition (4) will be automatically satisfied. It is this equivalent construct, that of a bipolar disk, that we shall have in mind in modelling the corrosion process.

Modelling in transformed coordinates

The cylindrical coordinate system, though simple and straightforward, is less felicitous for the present problem

than another orthogonal set: the oblate spheroidal coordinate system. The latter employs two dimensionless coordinates[1] η and ξ that are linked to the cylindrical coordinates through the equations [7]

$$r = a\left(1+\xi^2\right)^{1/2}\left(1-\eta^2\right)^{1/2} \tag{6}$$

and

$$z = a\xi\eta \tag{7}$$

where a is a reference length, that we set equal to the disk radius R. The third coordinate is of no concern in the present axisymmetric problem. Notice that when $z=0$, either $\xi=0$ and $\eta=\left(R^2-r^2\right)^{1/2}/R$, corresponding to a surface of the disk or $\eta=0$ and $\xi=\left(r^2-R^2\right)^{1/2}/R$, corresponding to the coplanar extension of the disk. Both coordinates are zero at the three-phase junction.

Figure 2 shows how the η and ξ coordinates index space in the geometry of interest. A surface of constant ξ is an oblate spheroid that obeys the equation,

$$\frac{r^2}{1+\xi^2}+\frac{z^2}{\xi^2}=R^2 \tag{8}$$

being generated by revolving an ellipse of semimajor axis $R\left(1+\xi^2\right)^{1/2}$ and semiminor axis $R\xi$, centred at the $z=r=0$ origin, about the $r=0$ axis. Values of ξ are limited to the range $\xi\geq 0$. A surface of constant η is generally spindle shaped, obeys the equation

$$\frac{r^2}{1-\eta^2}-\frac{z^2}{\eta^2}=R^2 \tag{9}$$

and is generated by revolving a hyperbola, centred at the origin, about the $r=0$ axis. The apex of the hyperbola lies on the disk at $r=R(1-\eta^2)^{1/2}$ and its asymptotes have a slope $\mathrm{d}z/\mathrm{d}r=\pm\eta/(1-\eta^2)^{1/2}$. Values of the η coordinate are confined to the range $-1\leq\eta\leq 1$ and we assign η a sign to match that of z. On the symmetry axis $r=0$, the spindle degenerates to a rod with η taking the value 1 above the disk and changing discontinuously to –1 below the disk. Typical spindles, with $0<\eta<1$ above the disk, suffer a similar discontinuity. The surface corresponding to $\eta=0$ is the entire $z=0$ plane, except for the disk.

We now need to restate the mathematical problem in the new coordinate system and for a bipolar disk electrode. In oblate spheroidal coordinates, Laplace's equation takes the form

$$\frac{\partial}{\partial\xi}\left[\left(1+\xi^2\right)\frac{\partial\phi}{\partial\xi}\right]+\frac{\partial}{\partial\eta}\left[\left(1-\eta^2\right)\frac{\partial\phi}{\partial\eta}\right]=0 \tag{10}$$

A solution to this equation is sought subject to the following conditions

$$\phi=\Phi,\xi=0,0<\eta<1 \tag{11}$$

[1]Alternatively, our ξ is often denoted $\sinh\{\xi\}$, our η being denoted $\sin\{\eta\}$.

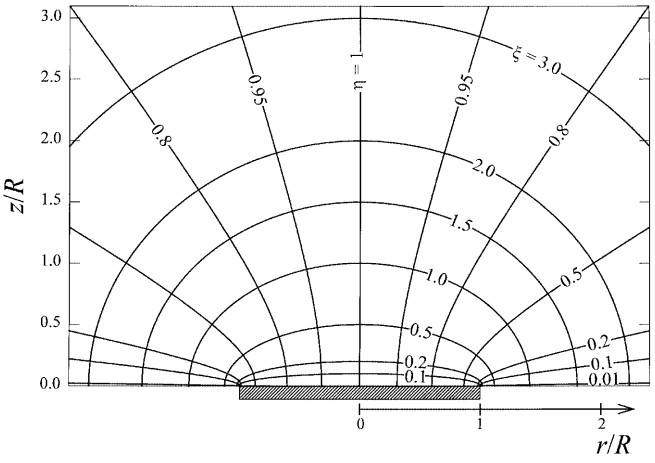

Fig. 2 The oblate spheroidal coordinate system used in the modelling of the corrosion

$$\phi=-\Phi,\xi=0,-1<\eta<0 \tag{12}$$

and

$$\phi=0,\eta=0,0<\xi<\infty \tag{13}$$

That

$$\phi\to 0,\xi\to\infty,-1\leq\eta\leq 1 \tag{14}$$

is evident from physical considerations.

The solution

Let it be postulated that, in oblate spheroidal coordinates, the Laplace equation is separable; that is, we assume [8] that

$$\phi(\xi,\eta)=F(\xi)G(\eta) \tag{15}$$

Subject to this assumption, Eq. (10) may be manipulated into

$$\frac{1}{F}\left[\left(1+\xi^2\right)\frac{\mathrm{d}^2F}{\mathrm{d}\xi^2}+2\xi\frac{\mathrm{d}F}{\mathrm{d}\xi}\right]=\frac{-1}{G}\left[\left(1-\eta^2\right)\frac{\mathrm{d}^2G}{\mathrm{d}\eta^2}-2\eta\frac{\mathrm{d}G}{\mathrm{d}\eta}\right] \tag{16}$$

Because the left- and right-hand sides of Eq. (16) are independent of η and ξ, respectively, each must equal the same constant, say k, that we take to be positive. Then

$$\left(1-\eta^2\right)\frac{\mathrm{d}^2G}{\mathrm{d}\eta^2}-2\eta\frac{\mathrm{d}G}{\mathrm{d}\eta}+kG=0 \tag{17}$$

follows from the right-hand side of Eq. (16).

The solution [9] of Eq. (17) is the simple expressions

$$G\{\eta\}=AP_v\{\eta\}+A'Q_v\{\eta\} \tag{18}$$

where $P_v\{\eta\}$ and $Q_v\{\eta\}$ are Legendre functions of the first and second kinds (see Chaps. 21, 59 in [10]), their degree, v, being related to the separation constant

by $\nu = (k + 1/4)^{1/2} - 1/2$. The multipliers A and A' are arbitrary constants which, since their values will reflect ν, we now denote A_ν and A'_ν. However, inasmuch as the Legendre functions of the second kind adopt infinite values at unity argument, $Q_\nu\{1\} = \infty$ irrespective of ν, the participation of this function would prevent the satisfying of condition (14) unless $A'_\nu = 0$, which assignment we therefore invoke. Moreover, the symmetry of our problem demands that ϕ be an odd function of η and this property is exhibited by Legendre functions of the first kind only if ν, which we henceforth replace by n, is an odd positive or an even negative integer. However, because $P_{-n-1}\{\eta\} = P_n\{\eta\}$, it will suffice to consider only $n = 1,3,5,....$ Because any odd integer will serve, the most general solution is

$$G\{\eta\} = \sum_{n=1,3}^{\infty} A_n P_n\{\eta\} \tag{19}$$

The allowed $P_n\{\eta\}$ functions are simple polynomials; for example, $P_1\{\eta\} = \eta$ and $P_3\{\eta\} = (5\eta^3 - 3\eta)/2$ and all vanish (see Table 1) at $\eta = 0$, ensuring that the boundary condition (13) is met.

With the separation constant k now replaced by its equivalent, $n(n+1)$, the left-hand side of Eq. (16) leads to

$$\left(1 + \xi^2\right)\frac{\mathrm{d}^2 F}{\mathrm{d}\xi^2} + 2\xi\frac{\mathrm{d}F}{\mathrm{d}\xi} - n(n+1)F = 0 \tag{20}$$

the form of which differs from Eq. (17) only in signs. The solution is analogous to Eq. (18), being in terms of $P_n\{\ \}$ and $Q_n\{\ \}$ functions, but this time of imaginary argument [11]

$$F\{\xi\} = B_n Q_n\{i\xi\} + B'_n P_n\{i\xi\} \tag{21}$$

For odd n, all $P_n\{i\xi\}$ functions are imaginary. Moreover, for odd $n > 1$, all $P_n\{i\xi\}$ functions approach infinity as $\xi \to \infty$, which would violate condition (14) unless all $B_n' = 0$. Therefore, we set each B' multiplier to zero. The $Q_n\{i\xi\}$ functions do not have these problems. Reassuringly, all $Q_n\{i\xi\}$ functions are real when n is an odd positive integer; for example, $Q_1\{i\xi\} = \xi\ \mathrm{arccot}\{\xi\} - 1$ and $Q_3\{i\xi\} = -[(5\xi^3 + 3\xi)/2]\ \mathrm{arccot}\{\xi\} + [(15\xi^2 + 4)/6]$. Moreover, such functions satisfy condition (14). Accordingly, we write

$$F\{\xi\} = \sum_{n=1,3}^{\infty} B_n Q_n\{i\xi\} \tag{22}$$

as the ξ-dependent portion of the solution.

By setting $C_n = A_n B_n/\Phi$, we see, on combining Eqs. (15), (19) and (22), that

$$\phi\{\xi,\ \eta\} = \Phi \sum_{n=1,3}^{\infty} C_n Q_n\{i\xi\} P_n\{\eta\} \tag{23}$$

It remains to identify the C_n multipliers. This is accomplished by satisfying the boundary conditions that apply on the disk, where $\xi = 0$. Table 1 contains an expression for $Q_n\{i0\}$when n is positive and odd. Substitution of this into Eq. (23) shows the potential on the disk to be

$$\phi\{0,\ \eta\} = \Phi \sum_{n=1,3}^{\infty} (-)^{(n+1)/2} \frac{(n-1)!! C_n P_n\{\eta\}}{n!!} \tag{24}$$

We use ( )!! to denote the semifactorial function (see Sect. 2:13 in [10]) defined, for odd n, by $(n-1)!! = (2)(4)(6)(...)(n-1)$ and $n!! = (3)(5)(7)(...)(n)$, it being understood that $(-1)!! = 0!! = 1!! = 1$.

Note from Eqs. (11) and (12) that, viewed as a function of η, ϕ displays a discontinuity at the $\xi = 0$ disk, changing as a step function from $-\Phi$ to Φ as η crosses zero. Just as such discontinuous functions can be represented as infinite Fourier series of sinusoids, so they can alternatively be represented as series of Legendre functions. It is demonstrated in Appendix A that the infinite series

$$\sum_{n=1,3}^{\infty} (-)^{(n-1)/2} \frac{(2n+1)(n-2)!! P_n\{\eta\}}{(n+1)!!} \tag{25}$$

has the property of representing a step function, equalling -1 for $-1 < \eta < 0$ and 1 for $0 < \eta < 1$. On

Table 1 Values of pertinent functions at special arguments when $n = 1,3,5,....$ Primes denote differentiation with respect to x or y. Where a general result is not available, a recursion formula is presented, together with the expressions needed to initiate the recursion. Some values reflect choices made in cutting the complex plane; our values relate to a single cut along the real axis from $-\infty$ to 1

Function	Value at $x = 0$ or $y = 0$	Values at $x = \pm 1$ or $y = \pm 1$
$P_{n-1}\{x\}$	$i^{n-1}(n-2)!!/(n-1)!!$	1
$P_n\{x\}$	0	± 1
$P_n'\{x\}$	$i^{n+1}n!!/(n-1)!!$	$n(n+1)/2$
$Q_0\{iy\}$	$\mp i\pi/2$	$\mp i\pi/4$
$Q_1\{iy\}$	-1	$(\pi/4) - 1$
$Q_{n-1}\{iy\}$	$i^n(n-2)!!\pi/2(n-1)!!$	Use $(n-1)Q_{n-1}\{\pm i\} = \pm(2n-3)iQ_{n-2}\{\pm i\} - (n-2)Q_{n-3}\{\pm i\}$
$Q_n\{iy\}$	$i^{n+1}(n-1)!!/n!!$	Use $nQ_n\{\pm i\} = \pm(2n-1)iQ_{n-1}\{\pm i\} - (n-1)Q_{n-2}\{\pm i\}$
$Q_0'\{iy\}$	i	$i/2$
$Q_1'\{iy\}$	$\pm\pi/2$	$\pm(\pi - 2)/4$
$Q_n'\{iy\}$	$i^{n-2}n!!\pi/2(n-1)!!$	Use $(n-1)Q_n'\{\pm i\} = \pm(2n-1)iQ_{n-1}'\{\pm i\} - nQ_{n-2}'\{\pm i\}$

equating each coefficient of $P_n(\eta)$ in series (25) with that in the summation in Eq. (24), one discovers that $C_n = -(2n+1)(n-2)!!n!!/(n-1)!!(n+1)!!$. Substitution of this result into Eq. (23) generates

$$\phi\{\xi,\ \eta\} = -\Phi \sum_{n=1,3}^{\infty} \frac{(2n+1)(n-2)!!n!!Q_n\{i\xi\}P_n\{\eta\}}{(n-1)!!(n+1)!!} \quad (26)$$

Thus Laplace's equation has been solved. An alternative solution has recently been published [6].

The potential distribution in solution

In general, we have not been able to sum the expression in Eq. (26) to create an analytical expression for the potential; however, using the software facilities of Mathematica [12], we were able to calculate[2] numerical values of $\phi\{\xi,\eta\}$. The method adopted to find pairs of (ξ,η) coordinates, and thence (r,z) pairs, corresponding to a chosen value of the ϕ/Φ ratio, is described in Appendix D. The results of such a numerical exercise are presented as the equipotential surfaces shown in cross section in Fig. 4.

On the symmetry axis, $r = 0$ or $\eta = 1$, Eq. (26) loses its $P_n\{\eta\}$ term because Legendre functions of the first kind invariably equal unity when their arguments are unity; therefore

$$\frac{\phi\{\xi,\ 1\}}{\Phi} = -\sum_{n=1,3}^{\infty} \frac{(2n+1)(n-2)!!n!!Q_n\{i\xi\}}{(n-1)!!(n+1)!!} \quad (27)$$

In Appendix B we demonstrate that this series has a simple algebraic sum, namely

$$\frac{\phi(\xi,\ 1)}{\Phi} = 1 - \frac{\xi}{\left(1+\xi^2\right)^{1/2}} \quad (28)$$

In terms of cylindrical coordinates, this means

$$\phi(0,z) = \Phi\left(1 - \frac{z}{(R^2+z^2)^{1/2}}\right) \quad (29)$$

which shows, for example, that the axial potential falls to about one-tenth of its value at the electrode surface, when z is close to the disk diameter $2R$. Evidently, the electrical perturbation of the solution, caused by the corrosion potential, is closely confined to the region of the inclusion. At larger distances, Eq. (29) is well approximated by $\phi = \Phi R^2/2z^2$, showing the inverse-square dependence that would be expected.

Figure 4 also shows the flux lines, the routes followed by the ions that sustain the corrosion current. These were constructed from the same data sets used to draw the equipotential surfaces, following the method described in Appendix D.

[2]In version 4.0, neither Mathematica's "LegendreP" function nor its equivalent "Hypergeometric2F1" function returns correct values invariably.

The current density on the electrode surfaces

Because the (ξ,η) system is orthogonal, a normal, of length n, to the electrode interface follows a line of constant η at the upper surface of the bipolar disk. Accordingly the current density at any point on the anode is given by

$$j(0,\ \eta) = -\kappa\left(\frac{\partial\phi}{\partial n}\right)_{\xi=0} = -\kappa\left[\frac{\partial\phi/\partial\xi}{\partial n/\partial\xi}\right]_{\xi=0} = -\kappa\frac{(\partial\phi/\partial\xi)_{\xi=0}}{R\eta} \quad (30)$$

where κ is the conductivity of the aqueous medium. In the final step $(\partial n/\partial\xi)$, the so-called scale factor h_ξ of the oblate spheroidal coordinate system, generally equal [13] to $a[(\xi^2+\eta^2)/(1+\xi^2)]^{1/2}$, was replaced in Eq. (30) by its value at $\xi = 0$. Substitution of the ξ-derivative of Eq. (26) into Eq. (30) yields

$$j\{0,\ \eta\} = \frac{\kappa\Phi}{R\eta}\sum_{n=1,3}^{\infty}\frac{i(2n+1)(n-2)!!n!!\left[Q_n'\{i\xi\}\right]_{\xi=0}P_n\{\eta\}}{(n-1)!!(n+1)!!} \quad (31)$$

where the prime on the $Q_n\{\ \}$ function represents differentiation with respect to the ξ coordinate.

On the $z = 0$ plane outside $r = R$, the roles of ξ and η are reversed. The normals there follow lines of constant ξ and accordingly the current density is

$$j(\xi,\ 0) = -\kappa\left(\frac{\partial\phi}{\partial n}\right)_{\eta=0} = -\kappa\left(\frac{\partial\phi/\partial\eta}{\partial n/\partial\eta}\right)_{\eta=0} = \kappa\frac{(\partial\phi/\partial\eta)_{\eta=0}}{R\xi} \quad (32)$$

In the final step the scale factor $h_\eta = (\partial n/\partial\eta)$, simply equal to $-a\xi$ when $\eta = 0$, was inserted. On evaluating the remaining derivative via Eq. (26), the result

$$j\{\xi,0\} = \frac{-\kappa\Phi}{R\xi}\sum_{n=1,3}^{\infty}\frac{(2n+1)(n-2)!!n!!Q_n\{i\xi\}\left[P_n'\{\eta\}\right]_{\eta=0}}{(n-1)!!(n+1)!!} \quad (33)$$

is obtained.

Derivatives of Legendre functions may be expressed as associated Legendre functions or alternatively, and more usefully in the present exercise, in terms of Legendre functions of changed and unchanged degree. Thus (Chap. 59 in [10])

$$P_n'\{\eta\} = \frac{-P_n^{(1)}\{\eta\}}{(1-\eta^2)^{1/2}} = \frac{n[P_{n-1}\{\eta\} - \eta P_n\{\eta\}]}{1-\eta^2} \quad (34)$$

and

$$Q'_n\{i\xi\} = \frac{Q^{(1)}_n\{i\xi\}}{\left(1+\xi^2\right)^{1/2}} = \frac{n[Q_{n-1}\{i\xi\} - i\xi Q_n\{i\xi\}]}{1+\xi^2} \tag{35}$$

From these relationships, or from Table 1, we can now obtain expressions for $[P'_n\{\eta\}]_{\eta=0}$ and $[Q'_n\{i\xi\}]_{\xi=0}$ to insert into Eqs. (33) and (31), respectively. The first insertion leads to the formula

$$j\{\xi,0\} = \frac{-\kappa\Phi}{R\xi}\sum_{n=1,3}^{\infty}\frac{(-)^{(n+1)/2}(2n+1)(n-2)!![n!!]^2 Q_n\{i\xi\}}{[(n-1)!!]^2(n+1)!!} \tag{36}$$

for the current density on the annulus. Similarly, the second insertion yields

$$j\{0,\,\eta\} = \frac{\pi\kappa\Phi}{2R\eta}\sum_{n=1,3}^{\infty}\frac{(-)^{(n-1)/2}(2n+1)(n-2)!![n!!]^2 P_n\{\eta\}}{[(n-1)!!]^2(n+1)!!} \tag{37}$$

for the current densities on the disk.

Of course, the current density at the centre of the disk is available by differentiation of Eq. (28). One finds

$$\left(\frac{\partial\phi}{\partial z}\right)_{r=0} = \frac{-\Phi R^2}{(R^2+z^2)^{3/2}} \tag{38}$$

and therefore

$$j(r=0,z=0) = -\kappa\left(\frac{\partial\phi}{\partial z}\right)_{r=z=0} = \frac{\kappa\Phi}{R} \tag{39}$$

This remarkably simple result for the current density at the centre of an anodic disk of radius R, when the cathode is the coplanar annulus, is to be compared with the value $2\kappa\Phi/\pi R$ for the current density at the centre of a similar disk embedded in an infinite coplanar *insulator*, when the cathode is a remote hemisphere [14]. We were surprised that, considering the much shorter electrical path in the present geometry, the central current density is enhanced by a mere 57%.

Sadly, the centre of the disk, $\xi=0$, $\eta=1$, is the only electrode site at which we have been able to determine the current density analytically; however, numerical values of the Legendre functions $P_n\{\eta\}$ and $Q_n\{i\xi\}$ are available from the Mathematica software [12]. Numbers from this source were used in a program exploiting the twin Eqs (36) and (37) to calculate the current density values listed in Table 2 and graphed in Fig. 3. No problems were encountered in implementing Eq. (36); however, even with modern aids, we experienced great difficulty in generating precise current densities via Eq. (37). The reason for this, and the method that we adopted to circumvent it, are explained in Appendix C.

Close to the axis, the current density is almost uniform but, as expected, the current density on the disk soon increases from $\kappa\Phi/R$ ever more steeply as one moves outwards from the centre, approaching an infinite positive value as the disk edge is neared. Of course, the infinite current density changes sign as $r=R$ is crossed and then falls precipitously in magnitude, declining towards zero as $r\to\infty$. The falloff is, in fact, as the *inverse cube* of the distance from disk's centre, being given by

$$j(\xi\to\infty,\ \eta=0) = \frac{-\kappa\Phi}{2R\xi^3} \approx \frac{-\kappa\Phi R^2}{2r^3} \tag{40}$$

when the radial distance r is large.

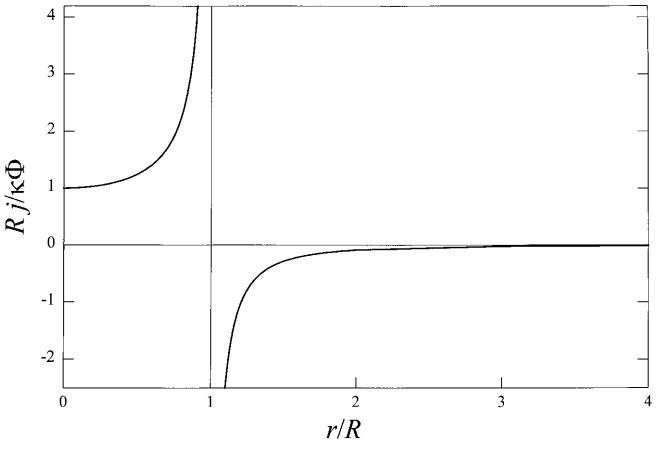

Fig. 3 The current density at the metal surface, plotted as a function of the radial distance from the disk's centre

Table 2 Normalized current densities, $j\{r,0\}$, at selected points on the anodic disk ($r<R$) and on the cathodic annulus ($r>R$)

r/R	ξ	η	$Rj\{\xi,\eta\}/\kappa\Phi$	r/R	ξ	η	$Rj\{\xi,\eta\}/\kappa\Phi$
0	0	1	1	1	0	0	$\pm\infty$
0.1	0	0.994987	1.008	1.001	0.044733	0	–316.9
0.2	0	0.9798	1.031	1.01	0.141774	0	–30.77
0.3	0	0.953939	1.074	1.05	0.320156	0	–5.583
0.4	0	0.916515	1.141	1.1	0.458258	0	–2.525
0.5	0	0.866025	1.246	1.2	0.663325	0	–1.065
0.6	0	0.8	1.411	1.5	1.118034	0	–0.2847
0.7	0	0.714143	1.692	2	1.732051	0	–0.08622
0.8	0	0.6	2.258	3	2.828427	0	–0.02114
0.9	0	0.43589	3.926	5	4.898979	0	–0.004188
0.95	0	0.31226	7.2	10	9.949874	0	–0.0005057
0.99	0	0.141067	32.9	20	19.9745	0	-6.268×10^{-5}
0.999	0	0.04471	319.7	50	49.99	0	-4.002×10^{-6}

Behaviour close to the hoop

The three phases – anode, solution and cathode – meet at the hoop where $\xi = \eta = 0$. Intuitively, we expect flux lines to be semicircular in this region, such that $(R–r)^2 + z^2$ is a constant for any particular flux line. Moreover, since such semicircles are parallel, one would expect that an ion following any one particular flux line would encounter a constant potential gradient. This argument leads to the conjecture that the equation

$$\phi(r \to R, z \to 0) = \phi(\xi \to 0,\ \eta \to 0) = \frac{2\Phi}{\pi}\arcsin\left(\frac{\eta}{\left(\xi^2+\eta^2\right)^{1/2}}\right) \tag{41}$$

should describe the potential close to the hoop. Numerical studies confirm that Eq. (41) is, indeed, valid. A consequence of this limiting equation is that equipotentials radiate linearly from the hoop, as Figs. 4 and 5 show. In cylindrical coordinates, the slopes of these limiting straight lines depend on the potential according to the formula

$$\frac{z}{r-R} = \tan\left(\frac{\pi\phi}{\Phi}\right) \tag{42}$$

For example $z = r–R$ when $\phi = \Phi/4$ and $z = R–r$ when $\phi = 3\Phi/4$; in each of these cases the equipotential surface is inclined at 45° to the metal surface as it reaches the hoop.

Consider an annulus of the anodic surface occupying $\rho < r < \rho + \mathrm{d}r$, where ρ is very close to, but slightly less than, R. The total area of this annulus will be $2\pi\rho\mathrm{d}r$. The ionic current leaving this annulus will flow along a semicircular current path of length $\pi(R–\rho)$ and arrive at a complementary cathodic annulus occupying $2R–\rho + \mathrm{d}r < r < 2R–\rho$, also of width $\mathrm{d}r$, outside the hoop as illustrated in Fig. 5. The current density will have a constant magnitude equal to the product of the conductivity and the potential gradient,

$$j\{\text{close to hoop}\} = \frac{-\kappa\mathrm{d}\phi}{\mathrm{d}\left[(R-r)^2+z^2\right]^{1/2}} = \frac{\kappa\phi}{\pi(R-\rho)} \tag{43}$$

at any point in the $(R–r)^2 + z^2 = (R–\rho)^2$ semicircle. Equation (43) gives the *magnitude* of the current density; its sign will be positive at $r = \rho$ and negative at $r = 2R–\rho$. This result predicts that $(R–r)j/\kappa\Phi$ will approach $1/\pi$ as $(R–r) \to 0$ and $–1/\pi$ as $(r–R) \to 0$. These predictions have been confirmed by numerical study of Eqs. (37) and (36), respectively. Indeed, since $1/(0.001)\pi$ equals 318.3, the symmetrical approaches are evident in Table 2.

Total corrosion current

At the outset of this research, we were uncertain as to whether the total current would turn out to be finite or infinite. The latter proves to be the case, as is easily demonstrated. As in the previous section, let ρ denote a value of r, smaller than R but sufficiently close that Eq. (43) can be taken to describe the current density. Not only does this confirm that the anodic current *density* at $r = R$ is infinite, but it also throws light on the size of the *total* corrosion current. Thus, we can evaluate the total anodic current as

$$I = 2\pi\int_0^R rj\{0,r)\mathrm{d}r = 2\pi\int_0^\rho rj\{0,r)\mathrm{d}r + 2\kappa\Phi\int_\rho^R \frac{r}{R-r}\mathrm{d}r \tag{44}$$

The second integral encounters a logarithmic infinity at its upper limit. Therefore, since both components of the final expression in Eq. (44) are positive, I must itself be positively infinite on the disk. And, of course, the annulus current must be negatively infinite.

Because all the current that originates on the anode arrives at the cathode, there is a one-to-one correspondence between any point on the disc and some point on

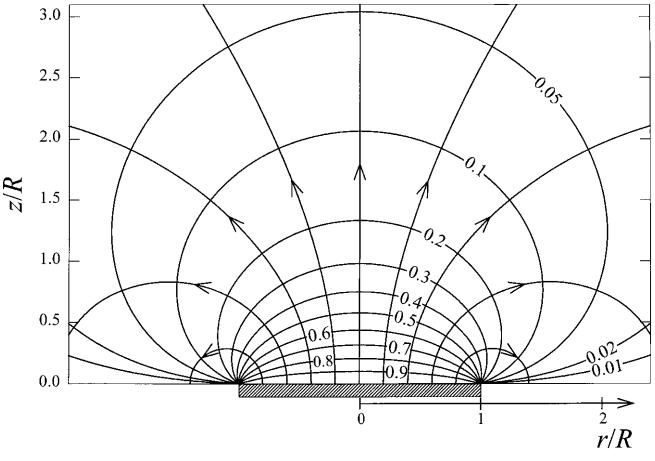

Fig. 4 Equipotential surfaces and flux lines (*arrowed*) shown in cross section

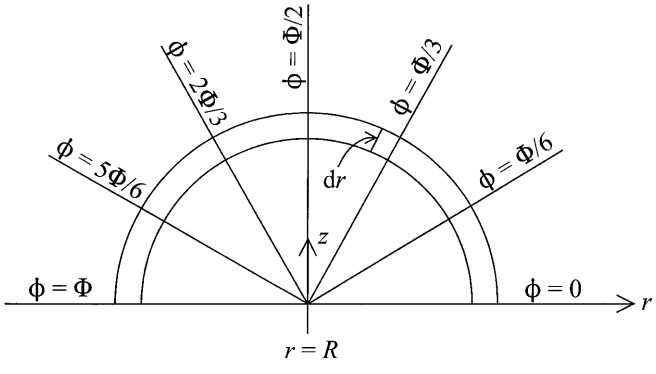

Fig. 5 Near the three-phase junction, $r = R$, $z = 0$, the flux lines are semicircular and the equipotential surfaces radiate from the hoop. A typical element through which ion transport occurs in the vicinity of the junction is shown

the cathode. Let r_c denote the radius of a circle on the cathode that is the sink of the current that has its source in the $r = r_a$ circle on the anode. Our earlier "semicircle" argument shows that, close to the hoop, the correspondence between r_c and r_a is

$$r_c + r_a = 2R \quad \text{close to the hoop.} \tag{45}$$

It is of interest to determine the equivalent relation for the current that originates close to the $r = 0$ axis of the anodic disk and that terminates on the distant reaches of the annulus. If r_c and r_a are a pair of radii that are complementary in this sense, it follows that the total currents from sources in $0 < r < r_a$ must be equal in magnitude to those ending at sinks in $r_c < r < \infty$. Accordingly

$$2\pi \int_0^{r_a} r j \mathrm{d}r = -2\pi \int_{r_c}^{\infty} r j \mathrm{d}r \tag{46}$$

Close to the axis, we know from Eq. (39) and Fig. 3 that the current density is very close to $\kappa\Phi/R$, while it is known from Eq. (40) that the current density far out on the annulus is $-\kappa\Phi R^2/r^3$. Insertion of these expressions for j into the corresponding integrals in equality (46) leads to the interesting resulting complementarity relationship

$$r_a^2 r_c = 2R^3 \quad \text{remote from the hoop} \tag{47}$$

after the integration is carried out. This relationship shows, for example, that current from $r = R/100$ terminates at the very large distance $r = 20{,}000R$.

Note added in proof

Since the submission of this article, Harold Levine (Stanford University, Calif.; private communication) has derived much more succinct formulas, namely

$$j\{r<R, 0\} = \frac{2\kappa\Phi R \mathrm{E}\{r/R\}}{\pi(R^2 - r^2)}$$

and

$$j\{r > R, 0\} = \frac{2\kappa\Phi r}{\pi}\left[\frac{\mathrm{K}\{R/r\}}{r^2} - \frac{\mathrm{E}\{R/r\}}{r^2 - R^2}\right]$$

as replacements for Eqs. (37) and (36), respectively. Here K{ } and E{ } are complete elliptic integrals (Chap. 61 in [10]). The normalized current densities in Table 2 prove to be in full agreement with corresponding values derived from these formulas.

Acknowledgements The financial support of the Natural Sciences and Engineering Research Council of Canada is acknowledged with gratitude. H. Levine, D. Livingstone-Bridge and an anonymous reviewer each kindly made valuable comments that have greatly improved this article. We also thank W.C. Topic, who helped with the preparation of the figures.

Appendix A

Legendre polynomials are orthogonal on the interval $-1 \le \eta \le 1$ with a weight function of unity. This implies that many functions $f\{\eta\}$ may be expressed on this interval by

$$f\{\eta\} = \sum_{m=0,1}^{\infty} c_m P_m\{\eta\} \tag{A1}$$

$$c_m = \frac{1}{\Omega_m}\int_{-1}^{1} f\{t\}P_m\{t\}\mathrm{d}t \tag{A2}$$

and

$$\Omega_m = \int_{-1}^{1} P_m^2\{t\}\mathrm{d}t = \frac{2}{2m+1} \tag{A3}$$

For the function of interest, in which $f\{\eta\}$ adopts the value -1 during $-1 < \eta < 0$ and 1 during $0 < \eta < 1$, Eq. (A2) becomes

$$c_m = (m + 1/2)\left[-\int_{-1}^{0} P_m\{t\}\mathrm{d}t + \int_{0}^{1} P_m\{t\}\mathrm{d}t\right] \tag{A4}$$

after Eq. (A3) is incorporated. For even degree m, Legendre polynomials are even functions and therefore their integrals cancel in Eq. (A4). Only the values $m = n = 1,3,5,...$ then need consideration, for which degrees the polynomials are odd, so that the integrals contribute equally and therefore

$$c_n = (2n+1)\int_0^1 P_n\{t\}\mathrm{d}t = \frac{(-)^{(n-1)/2}(2n+1)(n-2)!!}{(n+1)!!} \tag{A5}$$

the integral being a standard form (Eq. 21:10:7 in [10]). Insertion of this result into Eq. (A1) validates expression (25).

Appendix B

By writing out the first few terms of the series on the right-hand side of Eq. (27), it may be shown that

$$\frac{\phi\{\xi, 1\}}{\Phi} = -\left[\frac{3}{2}Q_1\{i\xi\} + \frac{21}{16}Q_3\{i\xi\} + \frac{165}{128}Q_5\{i\xi\} + \frac{2625}{2048}Q_7\{i\xi\} + \frac{41895}{32768}Q_9\{i\xi\} + \cdots\right] \tag{B1}$$

Legendre functions of the second kind, of odd degree and imaginary argument, may be expanded in inverse powers of their argument; thus (Chap. 12 in [8])

$$Q_n\{i\xi\} = \frac{1}{2}\left(\frac{-4}{\xi^2}\right)^{(n+1)/2} \sum_{j=0,1}^{\infty} \frac{(n+j)!(n+2j)!}{j!(2n+2j+1)!}\left(\frac{-1}{\xi^2}\right)^j \quad \text{(B2)}$$

If sufficient terms in the $n = 1,3,5,7$ and 9 versions of this formula are evaluated and substituted into expression (B1), one discovers, after considerable labour, that

$$\frac{\phi(\xi,\ 1)}{\Phi} = \frac{1}{2\xi^2} - \frac{3}{8\xi^4} + \frac{5}{16\xi^6} - \frac{35}{128\xi^8} + \frac{63}{256\xi^{10}} - \cdots \quad \text{(B3)}$$

The coefficients in this series may be recognized as binomial coefficients, leading to formula (28). This is an inelegant proof, but copious numerical evidence has also established the identity of the right-hand sides of Eqs. (27) and (28).

Appendix C

For odd n, the ratio $(n–1)!!/n!!$ approaches $(\pi/2n)^{1/2}$ as $n\to\infty$ (Eq. 2:13:6 in [10]). It follows that

$$\frac{(2n+1)(n-2)!![n!!]^2}{[(n-1)!!]^2(n+1)!!} \to \left(\frac{32n}{\pi^3}\right)^{1/2} \quad \text{(C1)}$$

in the same limit. Moreover [15]

$$P_n\{\cos\theta\} \to \left(\frac{2\csc\theta}{n\pi}\right)^{1/2} cos\{(n+1/2)\theta - \pi/4\} \text{ as } n \to \infty \quad \text{(C2)}$$

From these two limiting forms, one can demonstrate that the nth summand in the expression, Eq. (37), that we use to calculate $Rj\{0,\eta\}/\kappa\Phi$, acquires the limit

$$\frac{(-)^{(n-1)/2}(\pi/2\eta)(2n+1)(n-2)!![n!!]^2 P_n\{\eta\}}{[(n-1)!!]^2(n+1)!!} \to \frac{4}{\pi(1-\eta^2)^{1/4}\eta}(-)^{(n-1)/2}\cos\{n\theta+\psi\} \quad \text{(C3)}$$

as n tends to infinity. Here $\theta = \arccos\{\eta\}$, while ψ temporarily abbreviates $(2\theta–\pi)/4$. Evident in the limiting expression (Eq. C3) is the sinusoidal variation of the summand's value with n. This prevents convergence of the sum, impeding the straightforward evaluation of the expression in Eq. (37).

Let M be an integer large enough that only a small error is introduced on replacing all the summands in Eq. (37) beyond $n = 4M–3$ by the right-hand side of Eq. (C3), rather than the existing left-hand side. Then

$$\frac{Rj\{0,\eta\}}{\kappa\Phi} = \frac{\pi}{2\eta}\sum_{n=1,3}^{4M-3}\frac{(-)^{(n-1)/2}(2n+1)(n-2)!![n!!]^2 P_n\{\eta\}}{[(n-1)!!]^2(n+1)!!} + \frac{4}{\pi(1-\eta^2)^{1/4}\eta}\sum_m (-)^{2m-1}\cos\{(4M+4m-1)\theta+\psi\} \quad \text{(C4)}$$

where the second summation index, which temporarily runs over $m = 0,1/2,1,...,\infty$, is defined by $M + m = (n+1)/4$. Our attention in the remainder of this paragraph will focus on this second summation in Eq. (C4), that we denote by S. First the summands in S can be paired and combined

$$\begin{aligned} S &= \sum_{m=0,1/2}^{\infty}(-)^{2m-1}\cos\{(4M+4m-1)\theta+\psi\} \\ &= -2\sin\{\theta\}\sum_{m=0,1}^{u}\sin\{4(M+m)\theta+\psi\} \end{aligned} \quad \text{(C5)}$$

Notice that we have replaced the upper infinite limit by u; our interest is in the behaviour of S as $u\to\infty$. Next, we replace the m summation by use of the Euler–Maclaurin formula (Eq. 4:14:1 in [10])

$$\sum_{m=0,1}^{u} f(m) = -\frac{f(u)-f(0)}{2} + \sum_{p=0,2}^{\infty}\frac{B_p}{p!}\left[\left(\frac{\mathrm{d}^{p-1}f}{\mathrm{d}\mu^{p-1}}\right)_{\mu=u} - \left(\frac{\mathrm{d}^{p-1}\mathrm{f}}{\mathrm{d}\mu^{p-1}}\right)_{\mu=0}\right] \quad \text{(C6)}$$

where μ is a continuous variable replacing the discrete m. Here B_p denotes the pth Bernoulli number ($B_0 = 1$, $B_2 = 1/6$, $B_4 = -1/30$, $B_6 = 1/42$, ...). Note that the leading term in the p summation is the definite integral of $f\{\mu\}$. In our case $f\{\mu\} = \sin\{4(M+\mu)\theta+\psi\}$ whence, for even p, $\mathrm{d}^{p-1}f/\mathrm{d}\mu^{p-1} = -(-)^{p/2}(4\theta)^{p-1}\cos\{4(M+\mu)\theta+\psi\}$. However (Eq. 34:6:2 in [10])

$$\cot\{2\theta\} = 2\sum_{p=0,2}^{\infty}\frac{(-)^{p/2}B_p}{p!}(4\theta)^{p-1} \quad \text{(C7)}$$

so it follows from Eq. (C6) that

$$\begin{aligned} &\sum_{m=0,1}^{u}\sin\{4(M+m)\theta+\psi\} \\ &= -\frac{\sin\{4(M+u)ta+\psi\} - \sin\{4Mta+\psi\}}{2} \\ &\quad -\frac{\cot\{2ta\}[\cos\{4(M+u)ta+\psi\} - \cos\{4Mta+\psi\}]}{2} \end{aligned} \quad \text{(C8)}$$

With the help of trigonometric identities, Eqs. (C5) and (C8) may now be combined into

$$S = \frac{\sec\{\theta\}[\cos\{4(M+u)\theta+\psi-2\theta\} - \cos\{4M\theta+\psi-2\theta\}]}{2} \quad \text{(C9)}$$

We see that as $u\to\infty$ S is itself oscillatory; however, its value at $u = \infty$ can be associated with the mean of its oscillations. That is, we set

$$\begin{aligned} S &= \frac{-\sec\{\theta\}\cos\{4M\theta+\psi-2\theta\}}{2} \\ &= \frac{-\cos\{(4M-3/2)\ \arccos\{\eta\} - \pi/4\}}{2\eta} \end{aligned} \quad \text{(C10)}$$

On replacement of the second summation in Eq. (C4) by the expression for S given in Eq. (C10), one finds

$$\frac{Rj\{0,\eta\}}{\kappa\Phi} = \frac{\pi}{2\eta}\sum_{n=1,3}^{4M-3}\frac{(-)^{(n-1)/2}(2n+1)(n-2)!![n!!]^2 P_n\{\eta\}}{[(n-1)!!]^2(n+1)!!} - \frac{2}{\pi(1-\eta^2)^{1/4}\eta^2\cos\{(4M-3/2)\ \arccos\{\eta\}-\pi/4\}} \tag{C11}$$

This is the complicated expression that was used to generate the $j\{0,\eta\}$ values listed in Table 2. Successively larger values of M were employed until further increase no longer produced a significant effect.

Appendix D

To delineate an equipotential line we started at $(0,z_0)$, where z_0 is the value given by Eq. (28) for the chosen ϕ/Φ ratio, $(\phi/\Phi)_s$. To find the next point, a program was written to search along a small circle, centred at $(0,z_0)$ and of radius L equal to $R/50$ until a point (r_1,z_1) was found that gave a ϕ/Φ ratio acceptably close to $(\phi/\Phi)_s$. Then another search was made along another small circle of the same radius, but now centred at (r_1,z_1). And so on until the hoop was reached. The search for point (r_{n+1},z_{n+1}) was carried out via an angle θ that was initially set to $\theta_0 = \arctan\{(z_n - z_{n-1})/(r_n - r_{n-1})\}$. The coordinate pair $(r_n + L\cos\theta,\ z_n + L\sin\theta)$ was then converted to $(\xi,\ \eta)$ coordinates and used in Eq. (26) to generate a trial value $(\phi/\Phi)_0$ of the normalized potential. Next θ was incremented to θ_1 by an arbitrary addition of 1°, and the procedure was repeated, generating a changed value $(\phi/\Phi)_1$ of the ratio. For the third guess, the angle was adjusted via the $m=1$ case of the linear interpolation/extrapolation formula

$$\theta_{m+1} = \frac{\theta_{m-1}\left[(\phi/\Phi)_m - (\phi/\Phi)_s\right] + \theta_m\left[(\phi/\Phi)_s - (\phi/\Phi)_{m-1}\right]}{(\phi/\Phi)_m - (\phi/\Phi)_{m-1}}. \tag{D1}$$

This formula often produced a satisfactory result, $(\phi/\Phi)_2$. If not, θ was changed from θ_2 to θ_3, where θ_3 was generated by setting $m=2$ in formula (D1). This process was continued until (ϕ/Φ) was equal to $(\phi/\Phi)_s$ to within a factor of 10^{-7}. In this way, a file of values $(0,z_0)$, (r_1,z_1), (r_2,z_2),... was constructed for each chosen value of the ϕ/Φ ratio. These files were used to draw the equipotential lines shown in Fig. 4 by linearly connecting adjacent points. The same files were also used to construct flux lines.

The construction of the flux lines requires linking the equipotential contours by lines that are orthogonal to those contours. The process involves a stepwise location of the crossing points of one flux line with each of the equipotential contours. We shall use subscript α to denote the contour at which the crossing point is known; β will denote the contour at which the crossing point is sought. Thus (r_α, z_α) denotes the intersection point of a particular flux line with the α contour. Similarly $(\mathrm{d}z/\mathrm{d}r)_\alpha$ represents the contour's slope at that point, being the negative reciprocal of the slope of the flux line itself. Now, for it to be possible for a circular arc to be drawn orthogonally between points (r_α, z_α) and (r_β, z_β), one on each of two distinct lines, then it is necessary[3] that

$$h_{\alpha\beta} = \left[\left(\tfrac{\mathrm{d}z}{\mathrm{d}r}\right)_\beta + \left(\tfrac{\mathrm{d}z}{\mathrm{d}r}\right)_\alpha\right]\left[(r_\beta - r_\alpha)^2 - (z_\beta - z_\alpha)^2\right] + 2(r_\beta - r_\alpha)(z_\beta - z_\alpha)\left[\left(\tfrac{\mathrm{d}z}{\mathrm{d}r}\right)_\beta\left(\tfrac{\mathrm{d}z}{\mathrm{d}r}\right)_\alpha - 1\right] \tag{D2}$$

be zero, as can readily be demonstrated. This property was used to locate the (r_β, z_β) point, from known values of r_α, z_α and $(\mathrm{d}z/\mathrm{d}r)_\alpha$. To start the process of locating the crossing points for each flux line in Fig. 4, we selected a value of r_α on the equipotential contour at which $(\phi/\Phi)=1$, i.e. the surface $z=0$ of the anode, so that z_α and $(\mathrm{d}z/\mathrm{d}r)_\alpha$ are both zero. We then examined the next equipotential contour file (that for which $\phi/\Phi=0.9$) and calculated the value of $h_{\alpha\beta}$ for the pairs (r_1,z_1), (r_2,z_2), ..., (r_n,z_n), ..., (r_N,z_N), by setting $r_\beta = r_n$, $z_\beta = z_n$ and $(\mathrm{d}z/\mathrm{d}r)_\beta = (z_{n+1} - z_{n-1})/(r_{n+1} - r_{n-1})$ for $n=1, 2, 3, ..., N$. This survey was halted as soon as the sign of $h_{\alpha\beta}$ changed[4], say from $-Q_{N-1}$ to $+Q_N$, both Qs being positive. This change of sign signifies that the (r_β, z_β) intersection point lies between $(r_{N-1},\ z_{N-1})$ and $(r_N,\ z_N)$. Accurate values of r_β and z_β were then found from the interpolation formulas

$$r_\beta = \frac{Q_N r_{N-1} + Q_{N-1} r_N}{Q_{N-1} + Q_N} \quad \text{and} \quad z_\beta = \frac{Q_N z_{N-1} + Q_{N-1} z_N}{Q_{N-1} + Q_N} \tag{D3}$$

with $(\mathrm{d}z/\mathrm{d}r)_\beta$ being calculated by a similar interpolation. These three quantities then become the α data from which the β values on the next equipotential contour are calculated.

The flux line itself was drawn through consecutive pairs of points, i.e. from (r_α, z_α) to (r_β, z_β), by using the specially created cubic spline

[3] But not sufficient. There may occasionally be points that give a zero value to $h_{\alpha\beta}$ but which do not lie on the sought flux line. Extemporary measures must be taken to exclude these.

[4] The sign change is easily recognized by the product of two consecutive values of $h_{\alpha\beta}$ being negative. Rarely, this will occur without a zero crossing if $h_{\alpha\beta}$ encounters an infinity. Such a false root is easily distinguished from a true root by the large magnitude of the negative product.

$$z = \frac{(r-r_\beta)^2 z_\alpha + (r-r_\alpha)^2 z_\beta}{(r_\beta - r_\alpha)^2} + \frac{(r-r_\alpha)(r-r_\beta)^2}{(r_\beta - r_\alpha)^3}\left[(r_\beta - r_\alpha)z'_\alpha + 2z_\alpha\right] + \frac{(r-r_\alpha)^2(r-r_\beta)}{(r_\beta - r_\alpha)^3}\left[(r_\beta - r_\alpha)z'_\beta + 2z_\beta\right] \quad \text{(D4)}$$

Here z'_α and z'_β represent the slopes of the *flux lines* at points (r_α, z_α) and (r_β, z_β); for example, $z'_\alpha = -1/(\mathrm{d}z/\mathrm{d}r)_\alpha$, where $(\mathrm{d}z/\mathrm{d}r)_\alpha$ is the slope of the *equipotential contour* at point (r_α, z_α).

References

1. Scheffey C (1988) Rev Sci Instrum 59:787
2. Issacs JS, Davenport AJ, Shipley A (1991) J Electrochem Soc 138:390
3. Sargent DA (1997) Corros Prevent Control 44:91
4. He J, Johnston-Gelling V, Tallman DE, Bierwagen GP (2000) J Electrochem Soc 147:3661
5. He J, Johnston-Gelling V, Tallman DE, Bierwagen GP, Wallace GG (2000) J Electrochem Soc 147:3667
6. Livingstone-Bridge D, Myland JC, Oldham KB (2001) Electrochem Commun (in press)
7. Morse PM, Feshbach H (1953) Methods of theoretical physics. McGraw-Hill, New York
8. Arfken G (1970) Mathematical methods for physicists. Academic, New York
9. Lebedev NN (1972) Special functions and their applications. Dover, New York, p 213
10. Spanier J, Oldham KB (1987) An atlas of functions. Hemisphere, New York; Springer, Berlin Heidelberg New York
11. Moon P, Spencer DE (1961) Field theory for engineers. Van Nostrand, Princeton, chapter 10
12. Mathematica. Wolfram Research, Champaign
13. Spiegel MR (1968) Mathematical handbook. McGraw-Hill, New York, p 128
14. Oldham KB (1989) J Electroanal Chem 260:461
15. Abramowitz M, Stegun IA (1964) Handbook of mathematical functions with formulas, graphs and mathematical tables. National Bureau of Standards, Washington DC, p 336